A mechanistic investigation of two-electron reduction in phenylene-bridged bispyridiniums

Unfinished manuscript

Authors: Garrett A. Meek, Anthony Petty, Benjamin G. Levine, Tom Guarr

8.1 Introduction

The search for materials which efficiently convert sunlight into usable energy has launched a tandem effort to develop materials which can effectively store this energy. Energy storage is a critical step in solar energy conversion, since our energy demands continue at night when the sun is unavailable. One of the most cost-effective ways to store the energy harvested from sunlight is electrochemically, for example, in a battery.

While batteries vary greatly in their architecture and complexity, previous work has shown that the cell potential in most batteries is limited by the potential at the cathode[1]. Commonplace battery technologies use metals such as lead and lithium for the cathode. Lead is desirable due to its low cost, but requires extra safety precautions due to its toxicity and has a low energy density. Lithium is desirable due to its high energy density, but is much more expensive than lead. Their strengths and weaknesses demonstrate why a great deal of research has been directed toward the discovery of cathodic materials that offer a better compromise between cost and energy density.

One approach to the design of lower-cost cathodes is to use metal-free materials. In general, the energy densities of organic materials are lower than metal-containing materials, however one may systematically optimize the energy density of organic materials through the rational design of chemically intuitive and low-mass redox sites[2]. Multielectron redox processes[3], in which more than one electron is added or removed from a molecule within a single oxidation step, are another important means of increasing the energy density of organic materials.

There are many examples of metal-containing materials which exhibit multielectron redox mechanisms, but fewer organic materials.

Recently Fortage, et al.[2], showed that polyarylpyridinium electrophores, a class of organic molecules characterized by a pyridinium base, a phenyl group at the 4- position, and varying R- groups at the 2- and 6- positions (see Figure 1 for illustrative examples), exhibit a single-step two electron reduction. Their conclusions are interesting in consideration of previous work by Michl, et al.[4, 5], in which it was concluded that polyarylpyridiniums (under the name "extended viologen") exhibit separate one-electron reduction steps. The version of the compound discussed by Michl was a derivative of p-phenylene-bis-4,4'-(1-aryl-2,6-diphenylpyridinium), shown in Figure 1A, which possessed acetanilide (phenyl group with acetamide at the 4- position) instead of phenyl groups at the R and R' positions. It is expected that the acetamide (-$NHCOCH_3$) groups would impact the reduction mechanism. Fortage used a combination of cyclic voltammetry and electronic structure calculations to demonstrate that pyramidalization at the nitrogen atom in the extended viologen base (a single polyarylpyridinium, or half of the structure in Figure 1A), without acetamide, occurs after a single reduction of the molecule from the native state to the cationic state. Pyramidalization enables further reduction of the molecule at the same potential in either a single step or step-wise manner, depending upon steric factors. The reduction mechanism in these polyarylpyridiniums suggests that molecules with similar structural motifs may demonstrate a similar multielectron redox process.

In the present work we report on the spectroelectrochemistry, cyclic voltammetry, and electronic structure of a class of 1,3- and 1,4- phenylene-bridged bispyridiniums (PBBs, Figure 1). We demonstrate that 1,4- bridged PBBs exhibit a two-step, two-electron reduction mechanism similar to polyarylpyridiniums, featuring pyramidalization at nitrogen atoms upon the first

reduction of the molecule. This reduction results in a change from aromatic (dication) to quinoidal (neutral) electronic structure in the bridging phenylene and pyridinium rings. The aromaticity of the native dicationic state has been discussed previously by Michl[5], however to our knowledge there has been no exploration of the change in electronic structure that is observed upon reduction. After characterizing the electronic structure of the reduced states we aim to contribute further to the discussion of whether or not this class of compounds undergoes a single or two step two-electron reduction through a thorough investigation of the reduction mechanism. A proposed mechanism for the reduction of 1,4- and 1,3- PBBs is shown in Figure 2. Note the presence of unpaired electrons in the proposed mechanism for 1,3- PBBs (Figure 2C). Knowledge about the locations of unpaired electrons for each of the states during the reduction process would be valuable to the rational improvement of molecules for applications in energy storage. We will demonstrate that the reduction mechanism depends upon the electron-withdrawing character of R-groups on the pyridinium rings.

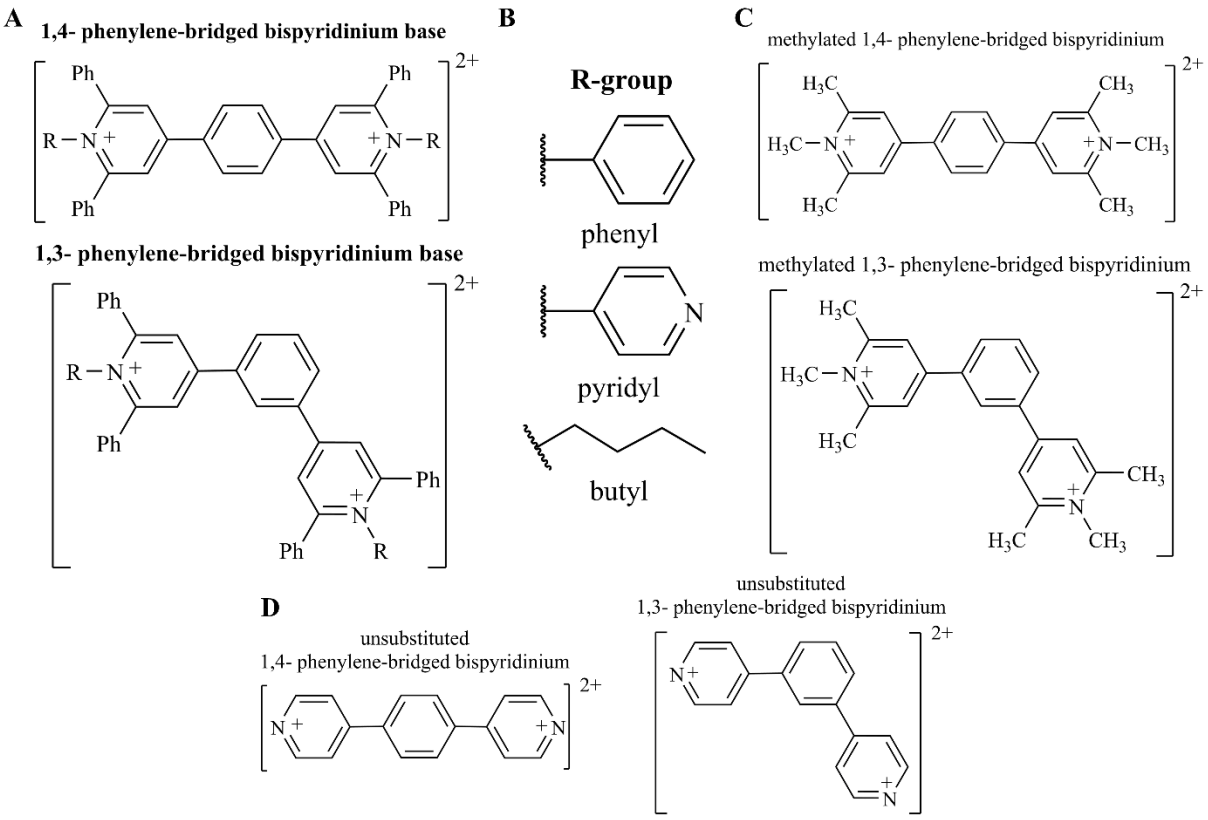

Figure 1: All systems discussed in the present study are shown in their native (dicationic) state. Molecules which were studied with both electronic structure and experimental approaches are listed in A, with R-groups listed in B.

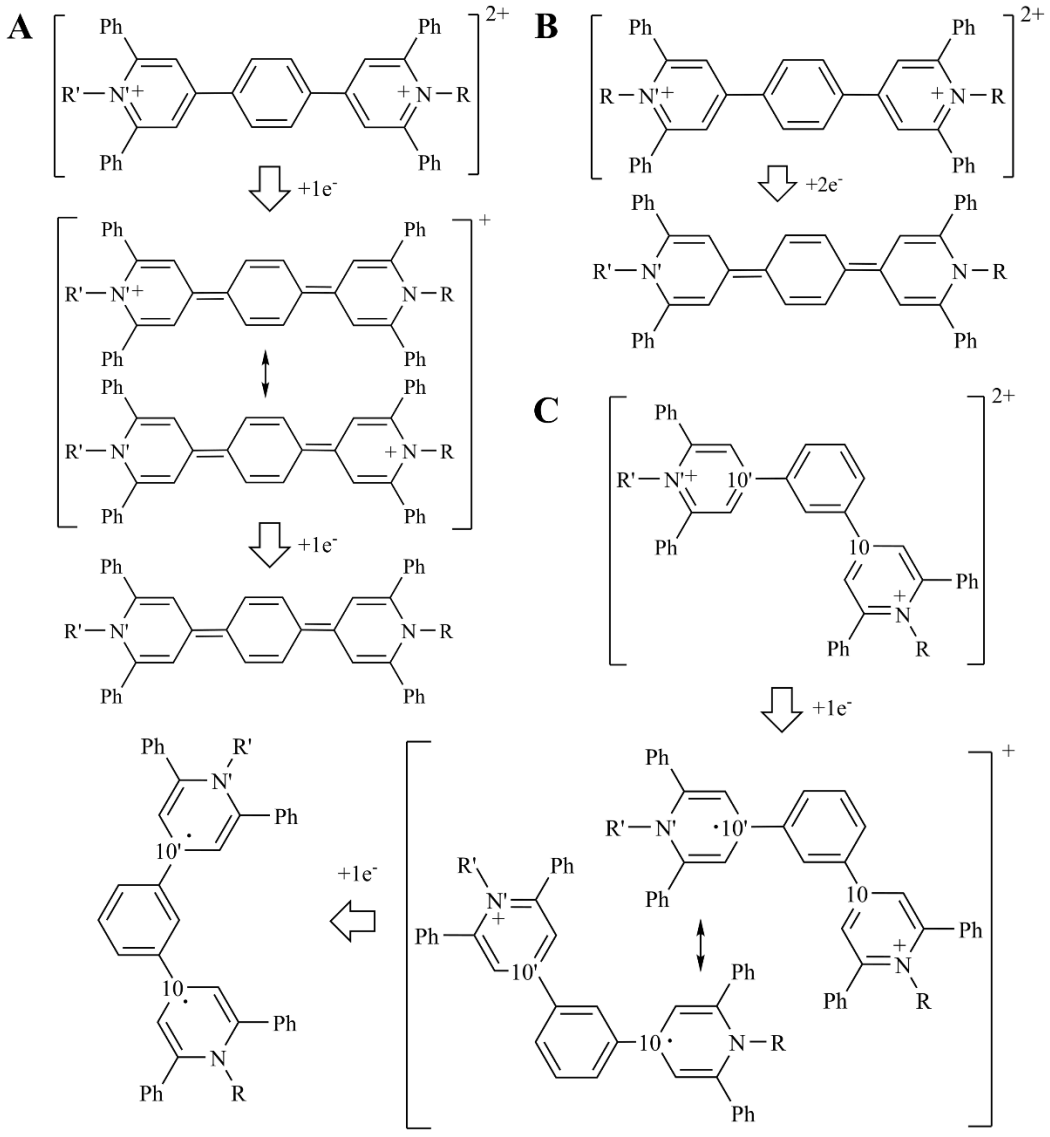

Figure 2: The proposed reduction mechanisms for 1,4- (A and B) and 1,3- (C) phenylene-bridged bispyridniums are shown. Note that for 1,4- bridged compounds two concurrent mechanisms are proposed. Atoms labeled "10" and "10'" are carbon atoms that are expected to accommodate unpaired electrons to facilitate quinoidal bonding in the 1,3- bridged pyridinium rings.

8.2 Methods

Cyclic voltammetry (CV) and spectroelectrochemistry data were generously provided and collected by Tom Guarr, et al., through a collaborative study. The synthesis and structural

characterization was also completed by Guarr, et al. Extensive discussion of synthetic details is omitted here due to the well-established synthetic approach[5], and the focus of the present work on the reduction mechanism and electronic structure. We note one difference from previous studies of structurally-related compounds: the CV and spectroelectrochemistry data in the present work were collected in propylene carbonate as a solvent, while previous studies of PBBs have primarily used acetonitrile. The 1,4- and 1,3- PBBs shown in Figure 1A, with all R-groups, were studied both experimentally and computationally. The methylated and unsubstituted compounds shown in Figures 1C and D were studied computationally in order to determine the effect of electron-withdrawing R-groups on the reduction mechanism and perform high-accuracy electronic structure calculations at a reasonable cost, respectively.

Due to the large computational cost of calculating the wave function for PBBs which, depending upon the R-groups, have as many as 460 electrons, we have optimized molecular structures computationally with the TeraChem graphical processing unit (GPU)-accelerated electronic structure software package[6-8]. All molecules were optimized with unrestricted density functional theory (U-DFT), the Coulomb-Attenuated B3LYP (CAM-B3LYP[9]) functional, which is expected to improve the treatment of long-range correlation effects in extended conjugated molecules, and the 6-31G** basis set.

In order to model the effects of propylene carbonate solvent on the reduction mechanism we have used the polarizable continuum model (PCM) [10, 11], as implemented in Q-Chem[12]. The PCM approach is an implicit solvent model which determines the free energy of solvation from electrostatic, dispersion-repulsion, and cavitation contributions. Q-Chem was also used for calculation of the Tamm-Dancoff approximation time-dependent DFT (TD-DFT) excitation energies and properties. A standard analysis of the character of these excitations would involve

visualization of either the Hartree-Fock or Kohn-Sham ground state orbitals with the largest amplitudes. Due to the complexity of some relevant excitations in PBBs we elect to observe the character of electronic excitations through the visualization of natural transition orbitals (NTOs)[13]. NTOs are obtained via an orbital transformation that combines a subset of ground state Hartree-Fock or Kohn-Sham orbitals into a set of particle-hole pairs, offering a compact and clear visual representation of a single particle-hole excitation. In most cases an excitation is well-characterized by a single particle-hole pair with an amplitude eigenvalue in the range of ~0.99.

In order to verify the proposed mechanism of 1,3- PBB reduction (Figure 2C) we have quantified the effective number of unpaired electrons (ENUE)[14, 15] for relevant atoms. The ENUE may be understood as a density matrix of unpaired electrons for the molecule, **D**, defined as:

$$\mathbf{D} = 2\mathbf{P} - \mathbf{P}^2, \tag{1}$$

where **P** is the spinless one-particle density matrix. The trace of **D** gives the ENUE on each atom in the molecule. We focus on analysis of the ENUE in 1,3- PBBs due to the proposed mechanism involving unpaired electrons at carbon atoms that connect the phenylene bridge. These carbon atoms are labelled 10 and 10' in Figure 2C.

The use of DFT, which may produce a range of values for the potential energy depending upon the chosen functional, encourages validation with higher-order electronic structure theories. The coupled cluster (CC) with single and double excitations (CCSD), equation of motion CCSD (EOM-CCSD)[16] and two-hole one-particle variant of the ionization potential EOM-CCSD (IP-(2*h*,1*p*)-EOM-CCSD)[17, 18] methods, as implemented[19-21] in GAMESS[22], were used for high-accuracy evaluation of the ground and excited state energies of unsubstituted 1,4- and 1,3-

PBBs (Figure 1D). These molecules were chosen due to the hypothesized importance of electron rearrangement in the phenylene bridge, and due to the prohibitive computational cost of CC calculations on molecules with substituted pyridinium rings. Comparison of TD-CAM-B3LYP and EOM-CC energies in these unsubstituted systems provides an indication of the accuracy of the TD-CAM-B3LYP excitation energies, character and state ordering in substituted systems.

8.3 Results

8.3.1 Does the two-electron reduction of PBBs occur in a single step?

Previous studies of phenylene-bridged bispyridiniums have featured a variety of R-groups. These R-groups may affect the reduction mechanism by either donating or withdrawing electrons from the phenylene-bispyridinium bridge. With some R-groups it has been claimed that the double reduction of the molecule is step-wise[4], while with other R-groups it has been claimed that the double reduction occurs in a single step[2]. Both studies provide compelling cyclic voltammetry measurements to support their arguments.

Figure 3 shows CV measurements for all experimentally studied PBBs. Note the differences between the peak spacing in the cases of 1,4- and 1,3- phenylene bridges. In the first case the CV shows a single cathodic peak for the double reduction of the molecule with all R-groups. This cathodic peak is followed by a second double reduction step from the neutral molecule to the dianion. Discussion of this second two-electron reduction step, however, is beyond the scope of the present work. Two energetically close but distinct cathodic peaks are clear in all 1,3- PBBs, while the distinction between the first and second cathodic peaks is most apparent in the case of the butyl-substituted molecule.

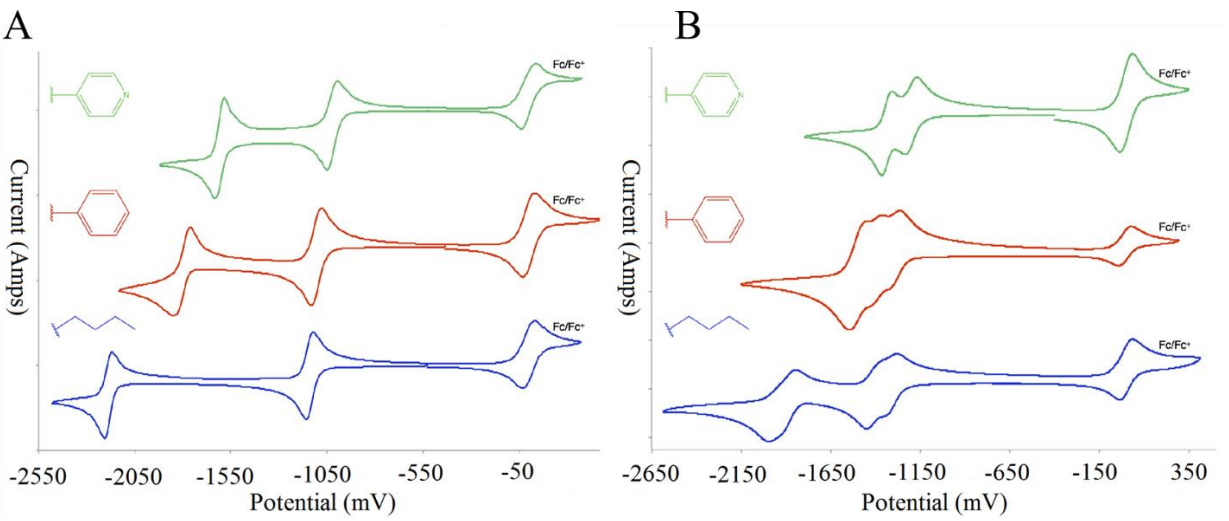

Figure 3: Cyclic voltammetry measurements (vs. Fc/Fc+, 0.2M $TEABF_4$ in MeCN) are presented for 1,4- and 1,3- PBBs (A and B, respectively). Note that the data has been shifted to more clearly distinguish the peaks for molecules with different R-groups, which are shown next to the data in their corresponding color.

These data suggest that the first two-electron reduction of PBBs occurs in a single step, while the first two-electron reduction of meta phenylene-bridged molecules occurs in two steps. Table 1 shows the PCM-DFT adiabatic electron affinities for the native and cationic states of all 1,3- and 1,4- PBBs. The only observable pattern in these electron affinities is that the second electron affinity is predicted to be smaller than the first. At first glance this result would appear to be in conflict with the CV data shown in Figure 3, which suggests that the 1^{st} and 2^{nd} electron affinities of 1,4- PBBs should be energetically closer. However, there are some experimental details that may partially explain this discrepancy. When collecting CV measurements, one's ability to distinguish cathodic peaks for energetically close but mechanistically distinct reduction steps is influenced strongly by the rate of change of the applied potential. In the opinion of our experimental collaborators, our ability to distinguish peaks in the CV would be improved by faster

sweeping rates. This would require more time and further experiments. Fortunately, spectroelectrochemistry may also be used to determine whether or not the cation is present in solution. This is another way of proving or disproving the hypothesis of single or two step two-electron reduction.

	1,4- bridged		**1,3- bridged**	
	+2→+1	+1→0	+2→+1	+1→0
methylated	3.04	2.57	2.80	2.59
R=phenyl	3.31	2.90	3.11	2.98
R=pyridyl	3.38	3.07	3.21	3.14
R=butyl	3.22	2.67	3.10	3.01

Table 1: PCM-DFT adiabatic electron affinities (in eV) for each of the compounds in the present study.

Figure 4 shows the spectroelectrochemical measurements of 1,4- and 1,3- PBBs with butyl R-groups. Plotted along with these measurements are Gaussian fits to the first ten excited states in the TD-CAM-B3LYP excitation spectrum. The spectrum for the 1,4- system exhibits a weak peak for the cation at 300 nm, with a stronger peak for the neutral molecule at 330 nm at open circuit voltage. When the applied potential is increased these peaks are slowly eliminated as the dication is formed. Note that the cationic and neutral peaks are almost indistinguishable for the 1,4- butyl-substituted system; this result demonstrates the advantage of a spectroelecrochemical analysis over CV analysis, in which the peaks were indistinguishable at slow sweeping rates. The 1,3- butyl-substituted molecule exhibits distinct absorption peaks at different applied potentials for the cationic and neutral molecule. In this case there is no question that the reduction mechanism is step-wise.

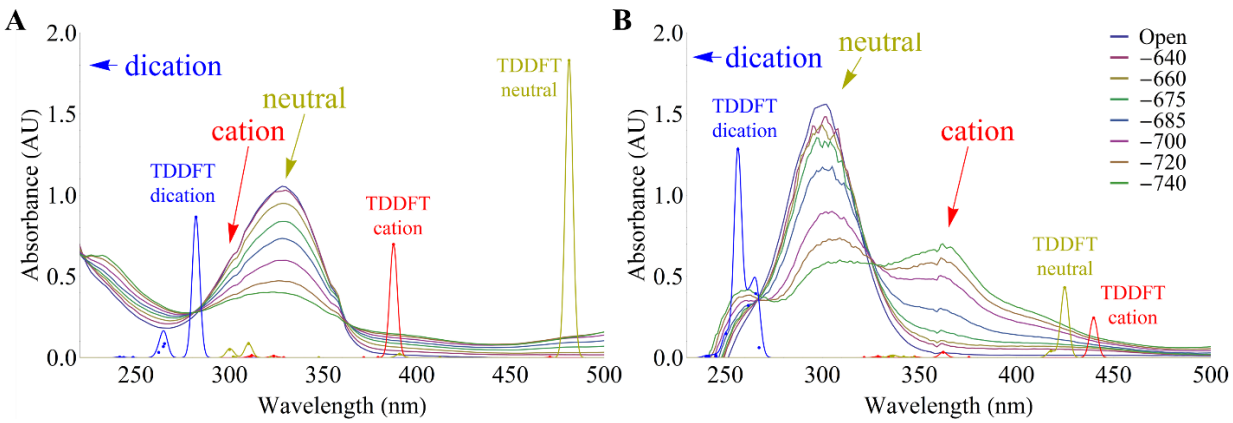

Figure 4: Spectroelectrochemistry data is presented for 1,4- (A) and 1,3- (B) PBBs with butyl R-groups. The legend for absorption curves at different applied potentials is shown at the right, where the units are mV. Overlaid on this data are Gaussian fits to the first ten excited states in the TD-CAM-B3LYP spectrum of the same molecules for each reduction state. Note that spectroelecrochemical absorption peaks due to the dication occur at lower wavelengths than are presented here, so that the spectra primarily illustrate the appearance of cationic and neutral peaks.

Although the TD-DFT excitation energies are significantly in error in comparison with spectroelectrochemical peaks for butyl-substituted systems, the relative absorptions and positions of the largest peaks in the TD-DFT spectrum aid in the interpretation of the spectroelectrochemical data. Note the agreement between the ratio of absorption peak heights for the cationic and neutral molecules using spectroelectrochemical and TD-DFT approaches in the 1,3- butyl-substituted molecule (Figure 4B). The ratio between these peak heights is 2.1 in spectroelectrochemical measurements and 1.8 in TD-DFT measurements.

We now return to the question at hand: does the two-electron reduction of 1,4- PBBs occur in a single step or step-wise? Comparison of the TD-DFT excitation peak heights and state

ordering with spectroelectrochemical data suggest that the small shoulder in the absorption spectrum of the 1,4- butyl-substituted molecule at 300 nm is the radical cation, but the data is inconclusive. Spectroelectrochemical data for phenyl-substituted 1,4- PBBs would aid in answering this question, and is shown in Figure 5. Note that in this spectrum there is no question about the presence of a radical cationic peak at 520 nm, whereas the neutral absorption spectrum has its maximum at 600 nm. The overlap between these spectral peaks with different applied potentials suggests that the energies of the first and second reduction are indeed comparable, but not identical. This is consistent with the DFT adiabatic electron affinities presented in Table 1.

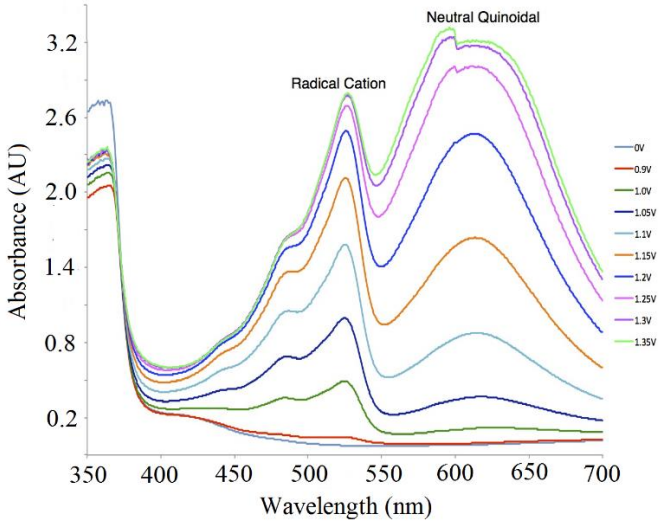

Figure 5: Spectroelectrochemical data is shown for 1,4- phenylene-bridged bispyridiniums. Note the presence of a radical cationic peak in the spectrum.

Figures 6-8 show the natural transition orbitals for the lowest energy bright excitation in the native (dication), cation, and neutral states for each molecule. Note that in all 1,4- PBBs (Figure 6), the lowest bright cationic and neutral excitations involve the same particle-hole pairs, where the particle orbital is a π-type orbital centered on the phenylene-bridged bispyridinium base, and the hole orbitals is a π*-type orbital also centered on the bridge. The ten lowest energy

excitation energies and oscillator strengths for these PBBs are listed in Tables 2-5. Quantitative agreement is not observed when comparing TD-CAM-B3LYP and experimentally gathered cationic and neutral excitation energies. As noted previously, however, comparing the ratio of the oscillator strengths of these states with spectroelectrochemical peak heights suggests that the TD-DFT excitation spectrum is qualitatively correct, by which we mean that it predicts the correct energetic ordering of the states that are relevant to the reduction mechanism, and qualitatively correct absorption features for their lowest bright excitations.

Figures 7 and 8 show the NTOs for the two lowest energy bright excitations in the meta-substituted compounds. Note that in most cases these two states involve particle-hole pairs that are localized on individual polyarylpyridiniums (R for one state and R' for the other). While one might expect the two lowest excitations in the meta-substituted compounds to be nearly degenerate in energy in the case of the cation, with similar oscillator strengths, TD-DFT predicts a gap of almost 1 eV between the lowest bright states in all of the cationic systems. The first bright cationic excitation is D_1, and the second bright state is the D_3. Comparison of the NTOs for the D_1 state show that the lowest energy excitation is a charge transfer excitation. The chemically unintuitive, and ultimately incorrect, description of the cationic excited state character and order in Tables 4 and 5 illustrates a well-known failing of TD-DFT in the description of charge transfer excited states[23, 24], which results from self-interaction error in the exchange correlation functional.

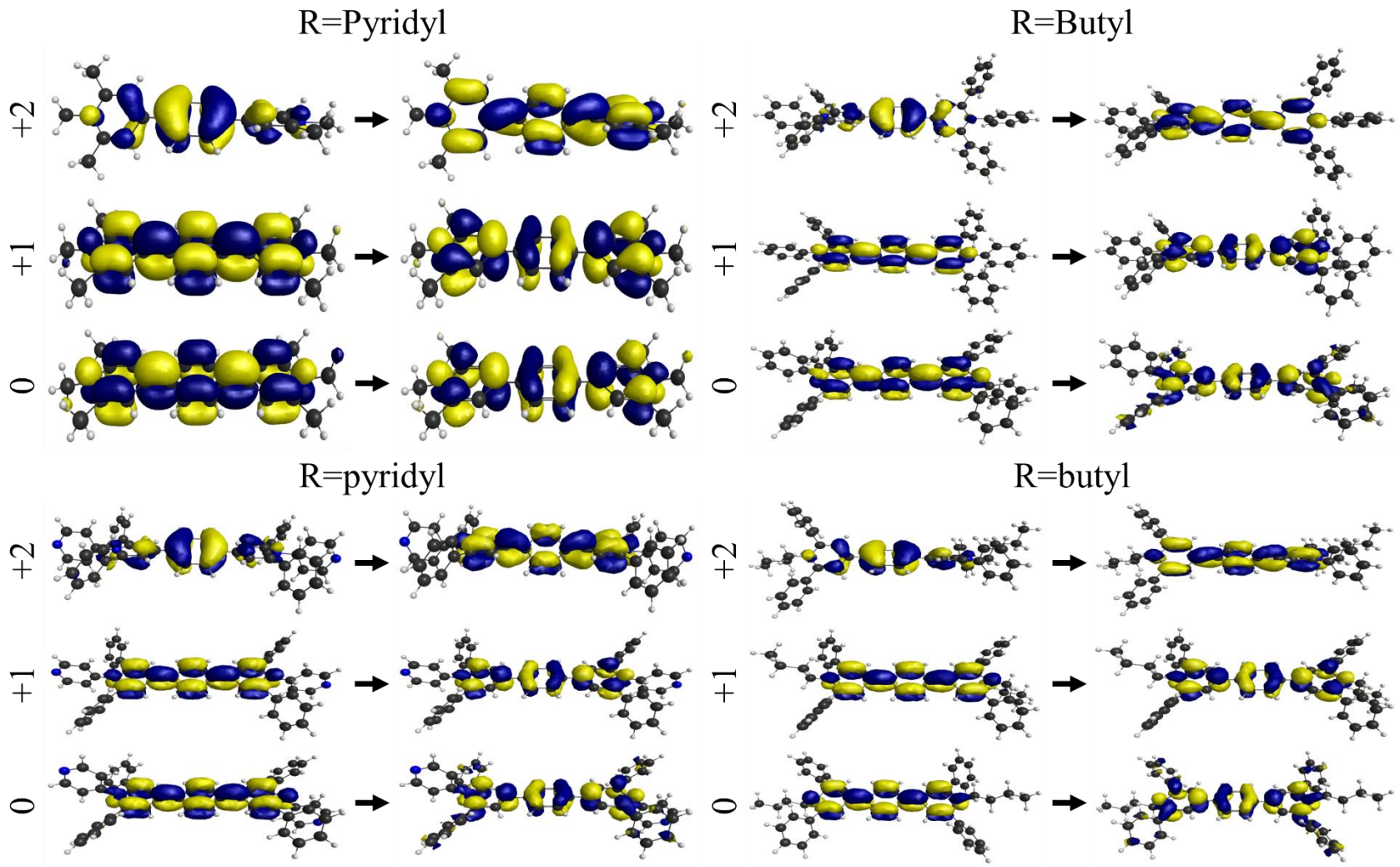

Figure 6: Natural transition orbitals (NTOs) are shown for the lowest energy bright excitation in each of the 1,4- bridged compounds. All dication excitations are from $S_0 \rightarrow S_1$, all cation excitations are from $D_0 \rightarrow D_1$, and all neutral excitations are from $S_0 \rightarrow S_1$.

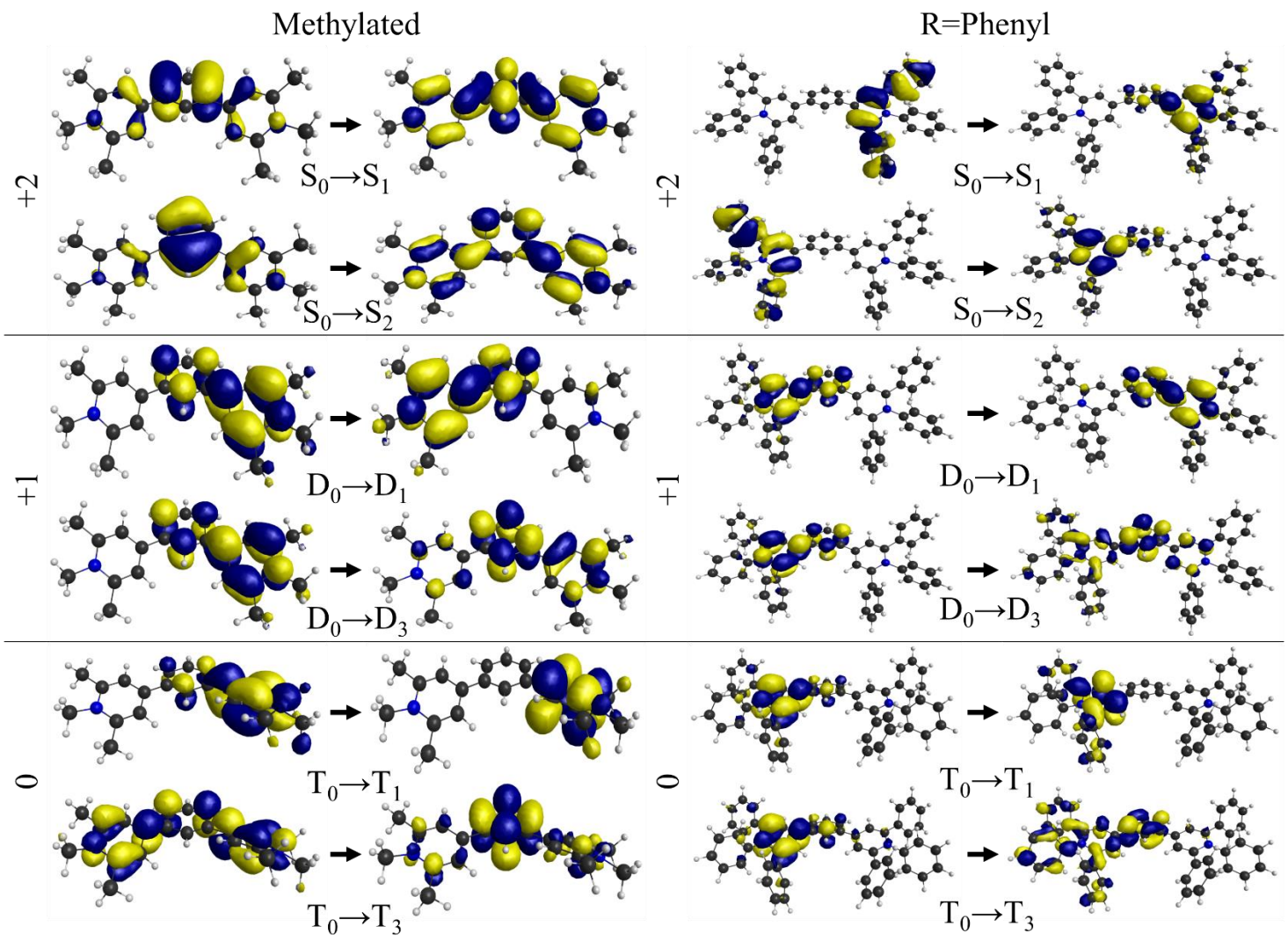

Figure 7: NTOs are shown for the two lowest energy bright excitations in the methylated and R=Phenyl 1,3- bridged molecules.

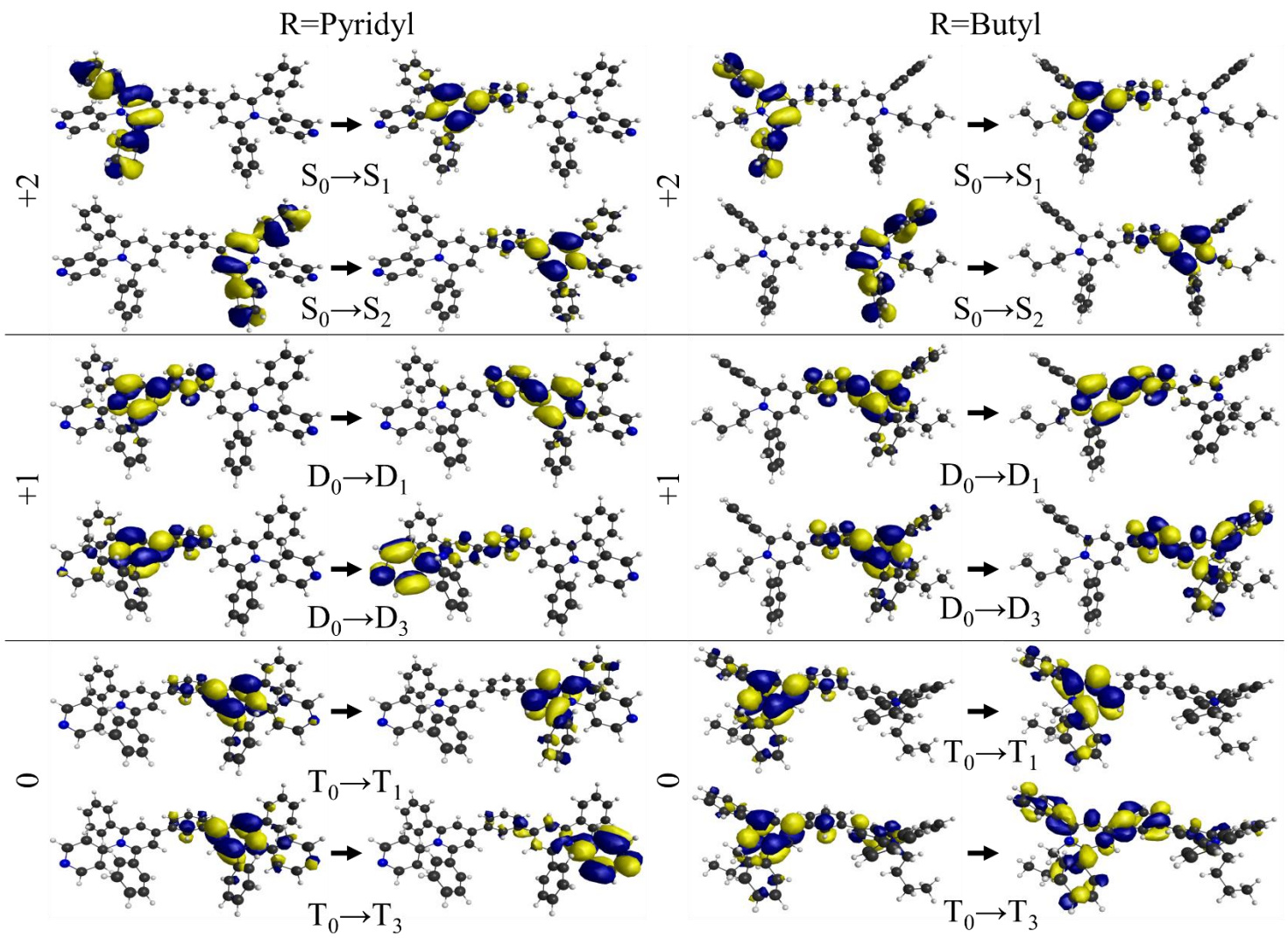

Figure 8: NTOs are shown for the two lowest energy bright excitations in the R=Pyridyl and R=Butyl 1,3- bridged molecules.

Methylated

Dication			Cation			Neutral		
State	Excitation Energy (eV)	*f*	State	Energy	*f*	State	Excitation Energy (eV)	*f*
S_1	4.57	1.35	D_1	1.65	0.74	S_1	3.01	3.45
S_2	4.82	0.01	D_2	2.57	0.00	S_2	3.04	0.00
S_3	5.16	0.12	D_3	2.88	0.00	S_3	3.41	0.00
S_4	5.17	0.14	D_4	3.31	1.28	S_4	3.88	0.00
S_5	5.46	0.00	D_5	3.34	0.00	S_5	4.36	0.00
S_6	5.93	0.00	D_6	3.50	0.00	S_6	5.17	0.00
S_7	6.31	0.00	D_7	4.07	0.00	S_7	5.61	0.00
S_8	6.38	0.00	D_8	4.18	0.00	S_8	5.67	0.00
S_9	6.51	0.06	D_9	4.30	0.00	S_9	5.84	0.04
S_{10}	6.58	0.12	D_{10}	4.35	0.07	S_{10}	5.93	0.00

R=Phenyl

Dication			Cation			Neutral		
State	Excitation Energy (eV)	*f*	State	Energy	*f*	State	Excitation Energy (eV)	*f*
S_1	4.29	1.76	D_1	1.44	0.98	S_1	2.55	3.86
S_2	4.40	0.23	D_2	2.40	0.00	S_2	2.93	0.00
S_3	4.41	0.51	D_3	2.55	0.01	S_3	3.04	0.05
S_4	4.42	0.00	D_4	3.21	1.48	S_4	3.69	0.00
S_5	4.43	0.17	D_5	3.26	0.00	S_5	3.91	0.00
S_6	4.69	0.03	D_6	3.30	0.00	S_6	3.94	0.00
S_7	4.91	0.00	D_7	3.79	0.00	S_7	3.95	0.00
S_8	4.91	0.01	D_8	3.87	0.00	S_8	4.29	0.19
S_9	4.93	0.01	D_9	3.89	0.00	S_9	4.32	0.04
S_{10}	4.93	0.01	D_{10}	3.92	0.04	S_{10}	4.32	0.00

Table 2: TDDFT vertical excitation energies and oscillator strengths (*f*, in a.u.) are shown for the 1,4- bridged methylated and R=Phenyl molecules.

R=pyridyl

Dication			Cation			Neutral		
State	Excitation Energy (eV)	*f*	State	Energy	*f*	State	Excitation Energy (eV)	*f*
S_1	4.31	1.69	D_1	1.49	0.93	S_1	2.56	3.85
S_2	4.43	0.00	D_2	2.47	0.00	S_2	2.86	0.00
S_3	4.45	0.57	D_3	2.62	0.00	S_3	2.94	0.04
S_4	4.65	0.03	D_4	3.21	1.48	S_4	3.59	0.00
S_5	4.87	0.00	D_5	3.32	0.00	S_5	3.64	0.01
S_6	4.87	0.00	D_6	3.35	0.00	S_6	3.72	0.00
S_7	4.90	0.00	D_7	3.40	0.00	S_7	3.93	0.00
S_8	4.90	0.00	D_8	3.46	0.00	S_8	4.10	0.05
S_9	4.96	0.00	D_9	3.82	0.00	S_9	4.18	0.00
S_{10}	4.96	0.01	D_{10}	3.91	0.02	S_{10}	4.33	0.18

R=butyl

Dication			Cation			Neutral		
State	Excitation Energy (eV)	*f*	State	Energy	*f*	State	Excitation Energy (eV)	*f*
S_1	4.40	1.73	D_1	1.49	0.89	S_1	2.58	3.66
S_2	4.68	0.17	D_2	2.46	0.00	S_2	3.01	0.00
S_3	4.69	0.14	D_3	2.63	0.00	S_3	3.18	0.04
S_4	4.73	0.07	D_4	3.20	1.39	S_4	3.57	0.00
S_5	4.99	0.00	D_5	3.27	0.00	S_5	3.86	0.00
S_6	5.00	0.00	D_6	3.34	0.00	S_6	4.00	0.17
S_7	5.10	0.00	D_7	3.77	0.00	S_7	4.09	0.00
S_8	5.10	0.00	D_8	3.84	0.02	S_8	4.11	0.01
S_9	5.14	0.00	D_9	3.98	0.03	S_9	4.11	0.01
S_{10}	5.14	0.01	D_{10}	3.99	0.00	S_{10}	4.14	0.10

Table 3: TDDFT vertical excitation energies and oscillator strengths (*f*, in a.u.) are shown for the 1,4- bridged R=Pyridyl and R=Butyl molecules.

Methylated

Dication			Cation			Neutral		
State	Excitation Energy (eV)	*f*	State	Energy	*f*	State	Excitation Energy (eV)	*f*
S_1	4.82	0.07	D_1	1.31	0.02	T_1	2.17	0.00
S_2	5.00	1.10	D_2	2.22	0.01	T_2	2.18	0.00
S_3	5.07	0.18	D_3	2.87	0.21	T_3	3.11	0.42
S_4	5.21	0.06	D_4	3.24	0.01	T_4	3.16	0.03
S_5	5.22	0.24	D_5	3.37	0.00	T_5	3.50	0.05
S_6	5.57	0.03	D_6	3.57	0.05	T_6	3.59	0.00
S_7	6.48	0.03	D_7	3.93	0.00	T_7	4.28	0.17
S_8	6.54	0.00	D_8	4.07	0.02	T_8	4.35	0.92
S_9	6.55	0.01	D_9	4.22	0.72	T_9	4.47	0.01
S_{10}	6.58	0.04	D_{10}	4.50	0.10	T_{10}	4.48	0.02

R=Phenyl

Dication			Cation			Neutral		
State	Excitation Energy (eV)	*f*	State	Energy	*f*	State	Excitation Energy (eV)	*f*
S_1	4.44	0.14	D_1	1.40	0.02	T_1	1.84	0.02
S_2	4.46	0.54	D_2	1.95	0.02	T_2	1.90	0.02
S_3	4.47	0.05	D_3	2.81	0.29	T_3	2.91	0.59
S_4	4.48	0.06	D_4	3.00	0.03	T_4	3.01	0.07
S_5	4.64	1.08	D_5	3.26	0.01	T_5	3.13	0.00
S_6	4.74	0.52	D_6	3.34	0.01	T_6	3.18	0.00
S_7	4.86	0.25	D_7	3.42	0.04	T_7	3.28	0.01
S_8	4.97	0.03	D_8	3.51	0.01	T_8	3.34	0.02
S_9	4.97	0.03	D_9	3.62	0.00	T_9	3.44	0.00
S_{10}	4.98	0.01	D_{10}	3.70	0.00	T_{10}	3.57	0.00

Table 4: TDDFT vertical excitation energies and oscillator strengths (*f*, in a.u.) are shown for the 1,3- bridged methylated and R=Phenyl molecules.

R=pyridyl

Dication			Cation			Neutral		
State	Excitation Energy (eV)	*f*	State	Energy	*f*	State	Excitation Energy (eV)	*f*
S_1	4.42	0.14	D_1	1.41	0.01	T_1	1.92	0.02
S_2	4.45	0.55	D_2	2.01	0.02	T_2	1.96	0.02
S_3	4.53	0.96	D_3	2.69	0.25	T_3	2.65	0.36
S_4	4.64	0.04	D_4	2.95	0.02	T_4	2.71	0.07
S_5	4.68	0.00	D_5	3.07	0.04	T_5	3.09	0.22
S_6	4.78	0.65	D_6	3.32	0.01	T_6	3.10	0.03
S_7	4.86	0.16	D_7	3.37	0.03	T_7	3.23	0.01
S_8	4.91	0.04	D_8	3.50	0.02	T_8	3.26	0.01
S_9	4.92	0.01	D_9	3.52	0.00	T_9	3.49	0.00
S_{10}	4.93	0.06	D_{10}	3.72	0.02	T_{10}	3.57	0.01

R=butyl

Dication			Cation			Neutral		
State	Excitation Energy (eV)	*f*	State	Energy	*f*	State	Excitation Energy (eV)	*f*
S_1	4.64	0.06	D_1	1.67	0.01	T_1	2.04	0.03
S_2	4.67	0.39	D_2	2.07	0.03	T_2	2.05	0.04
S_3	4.74	0.32	D_3	2.82	0.24	T_3	2.92	0.43
S_4	4.84	1.28	D_4	3.30	0.00	T_4	2.97	0.04
S_5	4.96	0.15	D_5	3.43	0.03	T_5	3.57	0.00
S_6	5.06	0.00	D_6	3.57	0.00	T_6	3.63	0.00
S_7	5.06	0.01	D_7	3.71	0.00	T_7	3.69	0.01
S_8	5.13	0.00	D_8	3.77	0.00	T_8	3.70	0.00
S_9	5.15	0.00	D_9	3.78	0.01	T_9	3.70	0.00
S_{10}	5.17	0.01	D_{10}	3.86	0.00	T_{10}	3.75	0.00

Table 5: TDDFT vertical excitation energies and oscillator strengths (*f*, in a.u.) are shown for the 1,3- bridged R=Pyridyl and R=Butyl molecules.

In principle, the CAM-B3LYP functional offsets this self-interaction error to some extent by incorporating a greater amount of Hartree-Fock exchange energy. The failing TD-DFT for some of the charge transfer states relevant to the present work will be analyzed and discussed further in Section 9.4 where the TD-DFT and IP-EOM-CCSD excitation energies and states are compared.

This section will be expanded, with a discussion of the other (Phenyl and Pyridyl) R-groups, once I get experimental data from Tom.

In summary, Figure 5 clearly demonstrates the presence of a cationic radical in the reduction pathway for 1,4- PBBs. What we have yet to address is the mechanism of this reduction. We now turn our attention to analysis of the reduction mechanism through the application of electronic structure theories.

8.3.2 Aromatic to quinoidal bond rearrangement in the double reduction of 1,4-phenylene-bridged bispyridiniums

The aromatic electronic structure of native (dication) 1,4- PBBs has been discussed previously by Michl, et al.[5]. This aromaticity is easily seen in the hole orbitals of the 1,4- PBBs in Figure 6. The quinoidal arrangement of the cationic and neutral states may also be easily visualized by the hole orbitals in Figure 6. We now further investigate the minimal energy molecular structures for each of these states to quantitatively confirm that the phenylene bridge is aromatically and quinoidally bonded in the dicationic and neutral states, respectively. In order to effectively discuss the structure of these molecules, which are large, complex and contain multiple R-groups, we have reduced their representation to a set of relevant atomic labels. These labels are

defined in Figure 9A, and are organized in order to allow a simple discussion of changes in PBB bond lengths.

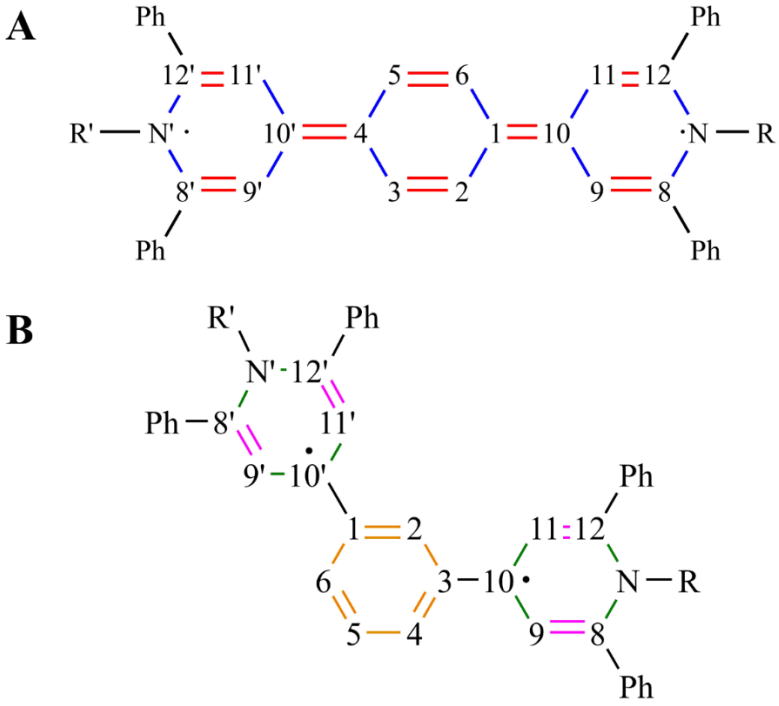

Figure 9: Atomic labels used for referencing bond lengths are defined for both 1,4- and 1,3- PBBs, with these molecules shown above in their neutral state. The same color labels are used in Figures 10 and 11 and Tables 6 and 7.

Figure 10 shows the bond lengths for red and blue bonds (see Figure 9 for color reference) in all reduced forms (dication, cation, neutral) of 1,4- PBBs. Additionally, the dihedral angles defined in Figure 9 are shown. These values are also organized for a more detailed comparison in Table 6. Comparison of the red bond lengths in Column A of Figure 10 shows that the red bonds are decreasing in length when the molecules are reduced from the native dicationic state to the neutral state. The expected C-C bond length for two carbons in a benzene ring is 1.40 Å, while

the expected lengths for single and double C-C bonds in general organic molecules are 1.54 and 1.34 Å, respectively. The native state bond length for the red bonds is, on average, 1.39 Å for the

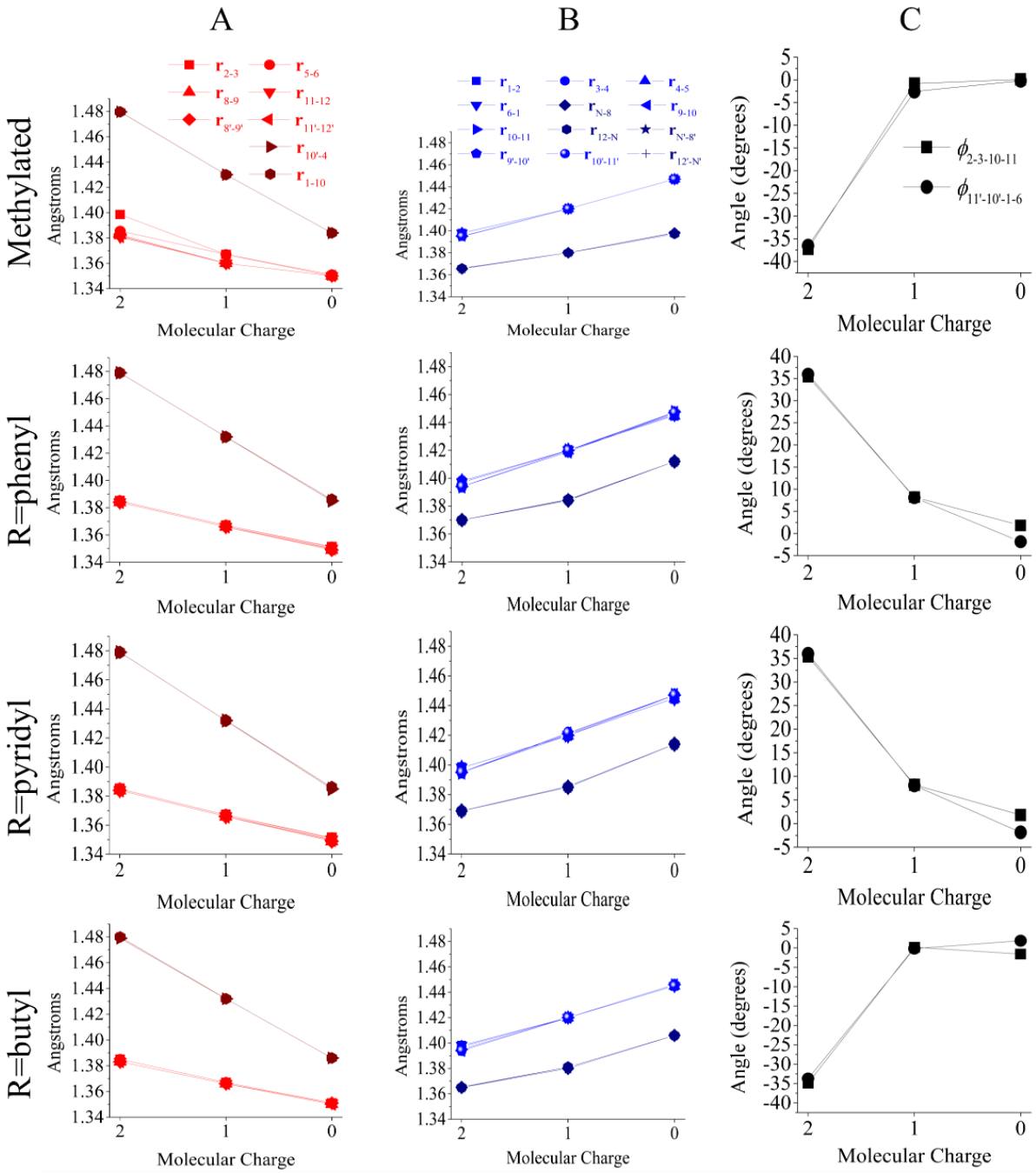

Figure 10: Bond lengths are plotted for the red (column A) and blue (column B) bonds in 1,4-bridged compounds, as defined in Figure 7A. The $\phi_{2\text{-}3\text{-}10\text{-}11}$ and $\phi_{11'\text{-}10'\text{-}1\text{-}6}$ dihedral angles are plotted in black in column C.

	methylated			R=phenyl			R=pyridyl			R=butyl		
	cation	neutral	dication	cation	cation	neutral	dication	cation	cation	neutral	dication	cation
$\mathbf{r}_{1\text{-}2}$	1.40	1.37	1.35	1.39	1.37	1.35	1.39	1.37	1.35	1.39	1.37	1.35
$\mathbf{r}_{2\text{-}3}$	1.40	1.42	1.45	1.40	1.42	1.45	1.40	1.42	1.45	1.40	1.42	1.45
$\mathbf{r}_{3\text{-}4}$	1.40	1.42	1.45	1.40	1.42	1.45	1.40	1.42	1.45	1.40	1.42	1.45
$\mathbf{r}_{4\text{-}5}$	1.40	1.42	1.45	1.40	1.42	1.45	1.40	1.42	1.45	1.40	1.42	1.45
$\mathbf{r}_{5\text{-}6}$	1.39	1.37	1.35	1.39	1.37	1.35	1.39	1.37	1.35	1.39	1.37	1.35
$\mathbf{r}_{6\text{-}1}$	1.40	1.42	1.45	1.40	1.42	1.45	1.40	1.42	1.45	1.40	1.42	1.45
$\mathbf{r}_{N\text{-}8}$	1.37	1.38	1.40	1.37	1.38	1.41	1.37	1.39	1.41	1.37	1.38	1.41
$\mathbf{r}_{8\text{-}9}$	1.38	1.36	1.35	1.38	1.37	1.35	1.38	1.36	1.35	1.38	1.37	1.35
$\mathbf{r}_{9\text{-}10}$	1.40	1.42	1.45	1.39	1.42	1.45	1.40	1.42	1.45	1.39	1.42	1.45
$\mathbf{r}_{10\text{-}11}$	1.40	1.42	1.45	1.39	1.42	1.45	1.40	1.42	1.45	1.40	1.42	1.45
$\mathbf{r}_{11\text{-}12}$	1.38	1.36	1.35	1.38	1.37	1.35	1.38	1.37	1.35	1.38	1.37	1.35
$\mathbf{r}_{12\text{-}N}$	1.37	1.38	1.40	1.37	1.38	1.41	1.37	1.39	1.41	1.37	1.38	1.41
$\mathbf{r}_{N'\text{-}8'}$	1.37	1.38	1.40	1.37	1.38	1.41	1.37	1.39	1.41	1.37	1.38	1.41
$\mathbf{r}_{8'\text{-}9'}$	1.38	1.36	1.35	1.38	1.37	1.35	1.38	1.37	1.35	1.38	1.37	1.35
$\mathbf{r}_{9'\text{-}10'}$	1.39	1.42	1.45	1.39	1.42	1.45	1.40	1.42	1.45	1.39	1.42	1.45
$\mathbf{r}_{10'\text{-}11'}$	1.39	1.42	1.45	1.39	1.42	1.45	1.40	1.42	1.45	1.39	1.42	1.45
$\mathbf{r}_{11'\text{-}12'}$	1.38	1.36	1.35	1.38	1.37	1.35	1.38	1.37	1.35	1.38	1.37	1.35
$\mathbf{r}_{12'\text{-}N'}$	1.37	1.38	1.40	1.37	1.38	1.41	1.37	1.39	1.41	1.37	1.38	1.41
$\mathbf{r}_{10'\text{-}4}$	1.48	1.43	1.38	1.48	1.43	1.39	1.48	1.43	1.39	1.48	1.43	1.39
$\mathbf{r}_{1\text{-}10}$	1.48	1.43	1.38	1.48	1.43	1.39	1.48	1.43	1.39	1.48	1.43	1.39
$\phi_{11'\text{-}10'\text{-}4\text{-}5}$	-37.23	-0.83	0.12	35.41	8.21	1.80	-34.66	-3.29	1.76	-34.93	0.19	-1.57
$\phi_{2\text{-}1\text{-}10\text{-}9}$	-36.54	-2.58	-0.19	35.97	8.09	-1.87	34.52	3.12	-1.80	-33.72	-0.16	1.86
$\phi_{R\text{-}N\text{-}12\text{-}11}$	-179.2	178.92	165.75	179.99	179.58	140.94	174.12	166.97	140.72	174.56	165.16	145.22
$\phi_{R'\text{-}N'\text{-}12'\text{-}11'}$	-178.45	177.51	166.75	179.88	179.48	141.36	174.19	167.61	140.29	174.99	165.86	145.76

Table 6: 1,4- PBB bond lengths (**r**, in Å), and dihedral angles (ϕ, in degrees) are shown.

bonds in the pyridinium rings and 1.48 Å for the bonds that bridge the phenylene. Bonds that bridge the phenylene are defined via atoms 1,4,10, and 10' by the variables $\mathbf{r}_{1\text{-}10}$ and $\mathbf{r}_{10'\text{-}4}$ in Figure 9, and are plotted in a darker red color in Figure 10 in order to better distinguish their behavior. In the neutral state, red bonds in the pyridinium rings have average lengths of 1.35 Å and $\mathbf{r}_{1\text{-}10}$ and $\mathbf{r}_{10'\text{-}4}$ have average lengths of 1.39 Å. This means that the average change in red bond lengths on the pyridinium rings is 0.04 Å, and 0.09 Å for the phenylene bridge. The bond lengths for the red bonds in the pyridinium rings of the neutral molecule are in good agreement with the expected bond length for a C-C double bond (1.34 Å). The blue bonds, which are expected to be single bonds in the neutral state, have a longer than expected average bond length of 1.44 Å (where the expected bond length for a C-C single bond is 1.54 Å). The lengths of bonds between nitrogen and carbon atoms in the pyridinium rings are distinguished through the use of a darker blue bond color, but little difference is observed between these and the lengths of the other blue bonds.

The dihedral angles of atoms that bridge the phenylene and pyridinium rings give a second indicator of the extent of aromaticity in the reduced state. In order for the molecule to have a quinoidal electron arrangement the dihedral angles $\phi_{11'\text{-}10'\text{-}4\text{-}5}$ and $\phi_{2\text{-}1\text{-}10\text{-}9}$ must be near 180º. In order for the molecule to have an aromatic electron arrangement the dihedral angles $\phi_{R\text{-}N\text{-}12\text{-}11}$ and $\phi_{R'\text{-}N'\text{-}12'\text{-}11'}$ must be near 180º. Column C in Figure 10 shows that $\phi_{11'\text{-}10'\text{-}4\text{-}5}$ and $\phi_{2\text{-}1\text{-}10\text{-}9}$ are, on average, 35º in the native state, and 0º in the neutral state. By contrast, $\phi_{R\text{-}N\text{-}12\text{-}11}$ and $\phi_{R'\text{-}N'\text{-}12'\text{-}11'}$ have an average value of 179º in the dicationic state and 148º in the neutral state. Comparison of the pyridinium and phenylene bridge dihedral angles thus demonstrates that their behavior is anti-correlated during the reduction process.

Structural differences between PBBs in their individual reduced forms may serve as a non-rigorous indicator of the energetic barrier for relaxing from one state to another. Analysis of the

dihedral angles, where the cationic and neutral angles are nearly identical and differ significantly from the dicationic dihedral angles, suggests that the first reduction is much less thermodynamically favorable than the second, since the bulk of the nuclear relaxation occurs in the first step when the molecule changes from aromatic to quinoidal. After this nuclear relaxation the accommodation of a second electron in the quinoidal hole orbital is much more thermodynamically favorable. This thermodynamic favorability is reflected in the difference between the first and second adiabatic electron affinities listed in Table 1. It also explains why cationic peaks are reliably observed in spectroelectrochemical measurements of 1,4- PBBs, but less reliably with CV measurements.

In summary, Figures 6 and 10 demonstrate that the electron arrangement in 1,4- PBBs changes from aromatic to quinoidal when they are reduced from their native state to the cationic and neutral states. We now discuss this result in the context of the reduction mechanism. Spectroelectrochemical measurements of 1,4- phenyl-substituted PBBs show a clear cationic absorption peak in addition to a larger neutral absorption peak, with some overlap between the two (see Figure 5). CV measurements suggest that the reduction steps are indistinguishable, at least with the sweeping rates we have yet obtained data for. The change from aromatic to quinoidal electronic structure in the first reduction step, as shown by the hole orbitals in Figure 6, provides important insight into the reduction mechanism, and explains the difficulty of experimentally distinguishing cationic and neutral species in solution.

8.3.3 Quinoidal bond arrangement and unpaired electrons in the reduction mechanism of 1,3- PBBs

The proposed mechanism for reduction of 1,3- PBBs (Figure 2C), hypothesizes a change from aromatic to quinoidal bonding when the first reduction occurs. This quinoidal bonding is facilitated by an unpaired electron at the 10 and 10' carbon atoms, as labeled in Figure 9B. Based upon this mechanism, bonds labeled in orange are not expected to exhibit significant changes in length when reducing from the native state to the neutral state, while the magenta bond lengths are expected to decrease and the green bond lengths are expected to increase with the formation of double and single bonds, respectively. The bond lengths for relevant atoms in the phenylene bridge are plotted for each reduced state in Figure 11, and organized for comparison in Table 7. As expected, the bonds in the phenylene bridge are asymmetrically stretched in the cationic state and then symmetric again in the neutral state (see orange colored plots in Column A of Figure 11). Comparison of magenta bond lengths for all compounds in Column B of Figure 11 shows that all decrease during reduction of the molecule, from an average initial value of 1.38 to 1.36 Å. This bond length is close to the expected length for a C-C double bond (1.34 Å), though the change during reduction is quite small. The green bonds (Column C in Figure 11) exhibit an average change in length of 0.04 Å, with an average initial length of 1.37 Å and final length of 1.41 Å. This is significantly smaller than the expected bond length for a single C-C bond. The combination of the green and magenta bond lengths in the neutral state suggests that the electron arrangement in neutral 1,3- PBBs is somewhere between aromatic and quinoidal, with bond lengths between the expected values for each of these electron arrangements.

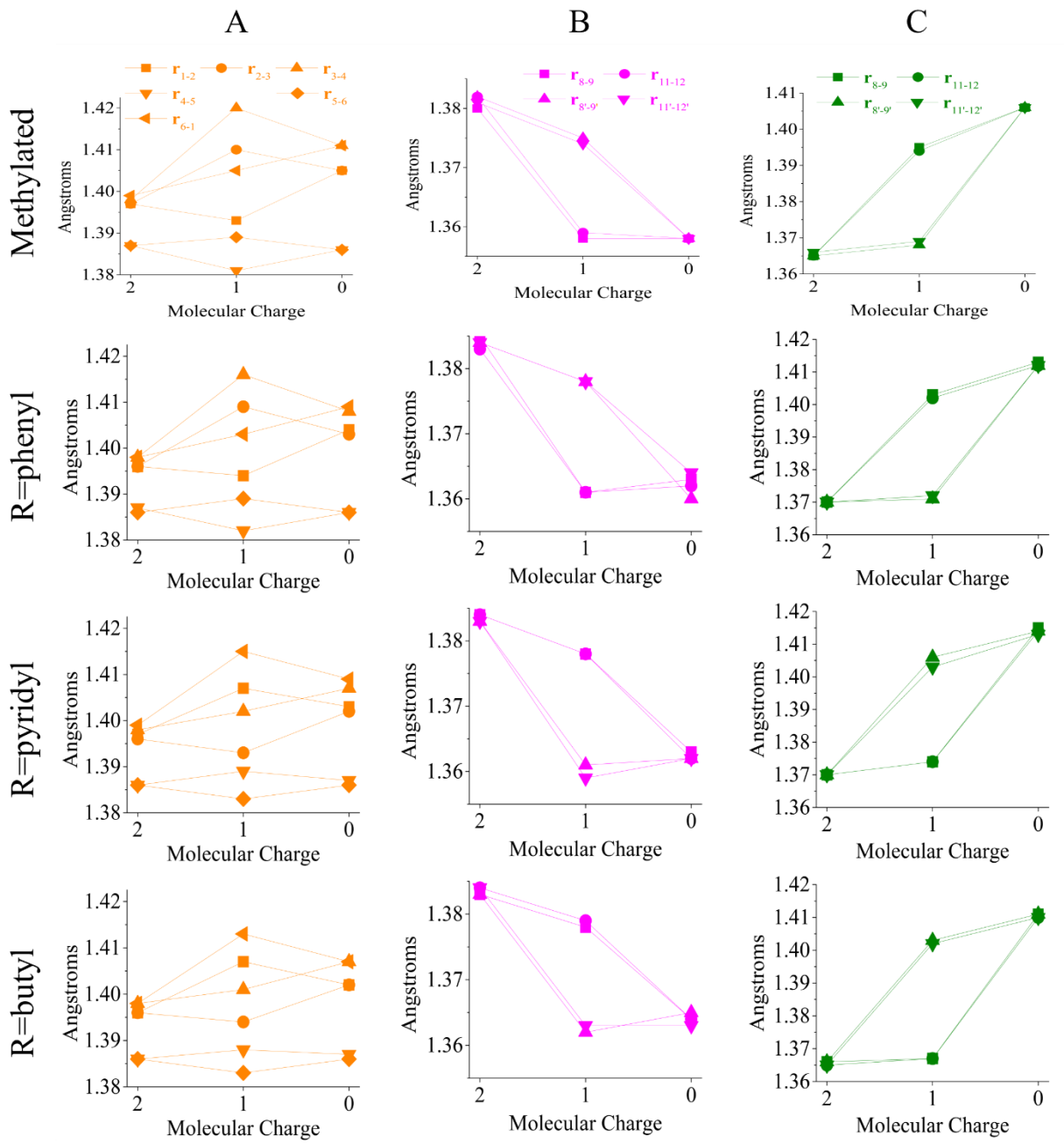

Figure 11: Bond lengths are plotted for the orange (column A), magenta (column B) and green (column C) bonds in 1,3- bridged compounds, as defined in Figure 7B.

	methylated			R=phenyl			R=pyridyl			R=butyl		
	dication	cation	neutral	dication	cation	neutral	dication	cation	neutral	dication	cation	neutral
$r_{1\text{-}2}$	1.40	1.39	1.41	1.40	1.39	1.40	1.40	1.41	1.40	1.40	1.41	1.40
$r_{2\text{-}3}$	1.40	1.41	1.41	1.40	1.41	1.40	1.40	1.39	1.40	1.40	1.39	1.40
$r_{3\text{-}4}$	1.40	1.42	1.41	1.40	1.42	1.41	1.40	1.40	1.41	1.40	1.40	1.41
$r_{4\text{-}5}$	1.39	1.38	1.39	1.39	1.38	1.39	1.39	1.39	1.39	1.39	1.39	1.39
$r_{5\text{-}6}$	1.39	1.39	1.39	1.39	1.39	1.39	1.39	1.38	1.39	1.39	1.38	1.39
$r_{6\text{-}1}$	1.40	1.41	1.41	1.40	1.40	1.41	1.40	1.42	1.41	1.40	1.41	1.41
$r_{N\text{-}8}$	1.37	1.40	1.41	1.37	1.40	1.41	1.37	1.37	1.42	1.37	1.37	1.41
$r_{8\text{-}9}$	1.38	1.36	1.36	1.39	1.36	1.36	1.38	1.38	1.36	1.38	1.38	1.36
$r_{9\text{-}10}$	1.40	1.43	1.42	1.39	1.42	1.42	1.39	1.40	1.42	1.40	1.40	1.42
$r_{10\text{-}11}$	1.40	1.43	1.43	1.39	1.42	1.42	1.39	1.40	1.42	1.39	1.40	1.42
$r_{11\text{-}12}$	1.38	1.36	1.36	1.38	1.36	1.36	1.38	1.38	1.36	1.38	1.38	1.36
$r_{12\text{-}N}$	1.37	1.39	1.41	1.37	1.40	1.41	1.37	1.37	1.41	1.37	1.37	1.41
$r_{N'\text{-}8'}$	1.37	1.37	1.41	1.37	1.37	1.41	1.37	1.41	1.41	1.37	1.40	1.41
$r_{8'\text{-}9'}$	1.38	1.38	1.36	1.38	1.38	1.36	1.38	1.36	1.36	1.38	1.36	1.37
$r_{9'\text{-}10'}$	1.40	1.40	1.42	1.39	1.40	1.42	1.40	1.42	1.42	1.40	1.42	1.42
$r_{10'\text{-}11'}$	1.40	1.40	1.43	1.39	1.40	1.42	1.40	1.42	1.42	1.39	1.42	1.42
$r_{11'\text{-}12'}$	1.38	1.37	1.36	1.38	1.38	1.36	1.38	1.36	1.36	1.38	1.36	1.36
$r_{12'\text{-}N'}$	1.37	1.37	1.41	1.37	1.37	1.41	1.37	1.40	1.41	1.37	1.40	1.41
$r_{10'\text{-}1}$	1.48	1.46	1.45	1.48	1.47	1.46	1.48	1.45	1.46	1.48	1.45	1.46
$r_{3\text{-}10}$	1.48	1.44	1.45	1.48	1.44	1.46	1.48	1.47	1.46	1.48	1.47	1.46
$\phi_{2\text{-}3\text{-}10\text{-}11}$	-38.02	-30.20	-20.33	36.05	30.97	17.70	-33.41	-12.81	-13.21	37.13	15.07	-16.93
$\phi_{11'\text{-}10'\text{-}1\text{-}6}$	38.82	13.11	-19.44	-38.40	-12.84	-22.30	40.65	28.53	21.73	-37.95	-31.16	-18.17
$\phi_{R\text{-}N\text{-}12\text{-}11}$	179.84	179.82	164.8	179.49	178.7	166.56	178.82	179.6	184.93	170.69	170.02	135.06
$\phi_{R'\text{-}N'\text{-}12'\text{-}11'}$	179.98	174.32	164.76	180.66	179.58	175.32	178.96	174.85	178.63	190.61	217.92	135.27

Table 7: 1,3- PBB bond lengths (**r**, in Å), and dihedral angles (ϕ, in degrees) are shown.

In 1,4- PBBs it was concluded that the bulk of the nuclear relaxation required to doubly reduce the molecule from its native state occurs in the first reductive step. This conclusion was drawn by comparison of the dicationic and cationic minimum energy structures, which indicate significant structural changes during the first reductive step and little change during the second step. The dihedral angles between the phenylene bridge and pyridinium rings, as well as the dihedral angles of the R-groups on the pyridinium rings, were found to correlate well with this proposal. In 1,3- PBBs these dihedral angles do not provide the same intuitive explanation for the energetic differences between the first and second reduction steps, though they do provide interesting insight into the stereochemistry.

9.4 Comparison of coupled cluster and DFT energies and excitation character for unsubstituted PBBs

The excitations shown in Figures 6-8 largely involve the phenyl-bridged bispyridinium bases (Figure 1D), and suggest that analysis of the accuracy of DFT in comparison with higher-accuracy electronic structure theories in these systems would give an indication of the accuracy of DFT energies for substituted PBBs. Table 10 compares energetic quantities of interest in the present study for the CC and DFT approaches. In both the 1,4- and 1,3- molecules the DFT first adiabatic electron affinities are significantly higher than those predicted by CC, with errors of 0.426 and 0.528 eV, respectively. By contrast, the DFT second adiabatic electron affinity is lower than the CC electron affinity. These discrepancies are a direct reflection of the complexity of the electronic structure of the cationic state, and the difficulty for DFT in describing this electronic structure. Although the values obtained for the first and second adiabatic electron affinities are in poor agreement, the sums of these values, which reflect the accuracy of the energy gap between

the neutral and dicationic minima, are in good agreement. With CC the sum of the first and second adiabatic electron affinities is 11.59 eV, while it is 11.77 for DFT. Agreement between DFT and CC methods on the sum of these quantities suggests that disagreement in the electron affinities is caused by an inaccurate cationic state energy.

The issues of DFT in describing the cationic state are further observed when visualizing the orbitals involved in the lowest energy bright excitations of unsubstituted PBBs, shown in Figure 16. In general, the CC and DFT methods are in good agreement on the character of these excitations. In the case of the 1,3- cation, however, there is a clear difference in the character of the orbitals that are involved in the excitation. The cationic excitation orbitals for the 1,3- molecule show a clear charge-transfer character, with electronic density located on different

	1,4- unsubstituted			1,3- unsubstituted	
	IP-EOM/EOM-CCSD	TD-CAM-B3LYP		IP-EOM/EOM-CCSD	TD-CAM-B3LYP
1st adiabatic electron affinity	7.254	7.680	1st adiabatic electron affinity	6.746	7.274
2nd adiabatic electron affinity	4.346	4.091	2nd adiabatic electron affinity	4.635	4.490
Dication ($S_0 \rightarrow S_1$) energy	4.596	4.386	Dication ($S_0 \rightarrow S_1$) energy	4.968	4.524
Cation ($D_0 \rightarrow D_1$) energy	2.836	1.664	Cation ($D_0 \rightarrow D_1$) energy	5.319	0.405
Neutral ($S_0 \rightarrow S_1$) energy	3.264	2.991	Neutral ($T_0 \rightarrow T_1$) energy	1.836	2.007
$S_0 \rightarrow T_1$ gap	0.476	0.280			

Table 10: IP-EOM/EOM-CCSD and TD-CAM-B3LYP energetic quantities (all in eV) are reported for unsubstituted 1,4- and 1,3-PBBs.

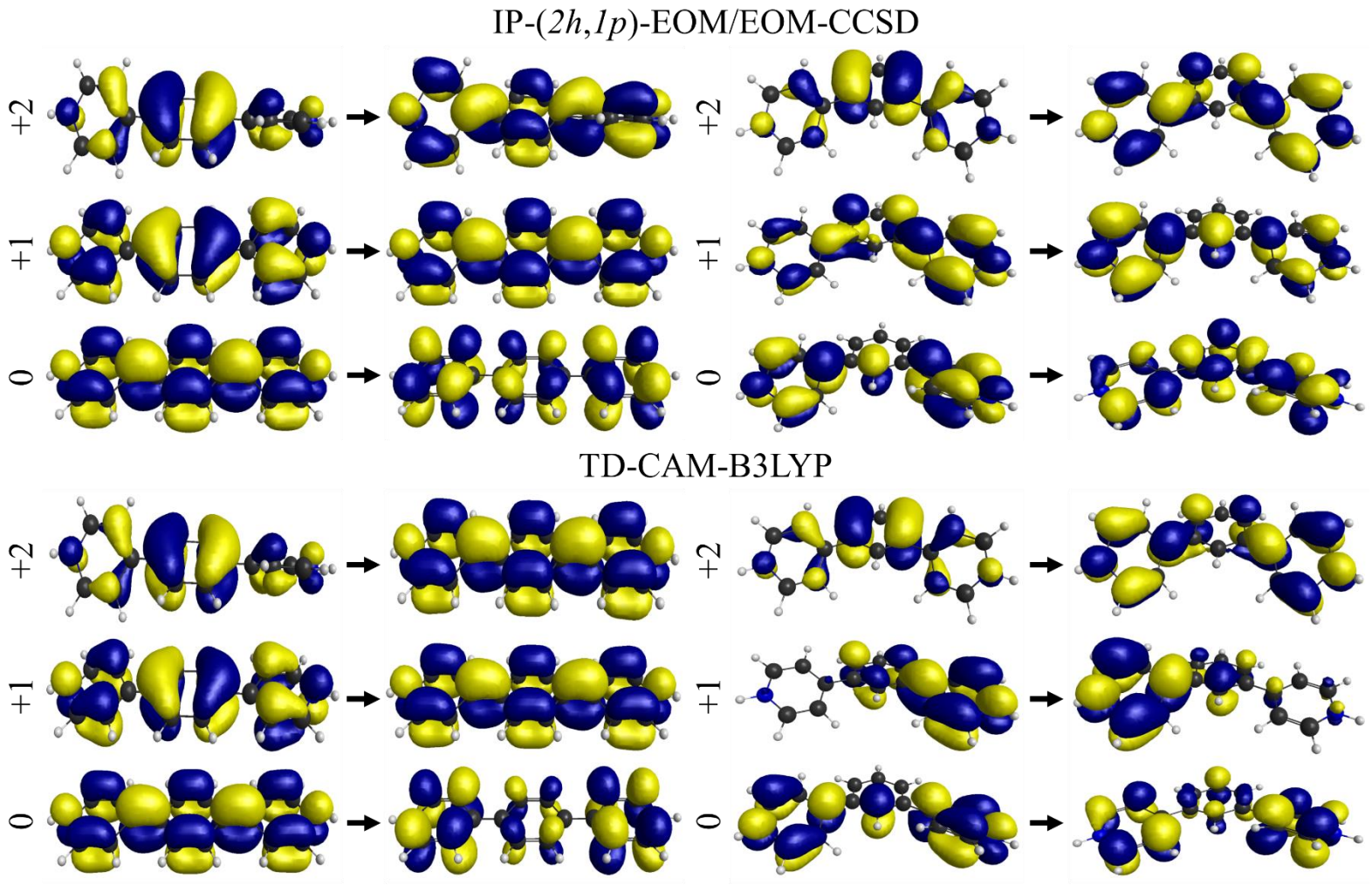

Figure 16: The Hartree-Fock and Kohn-Sham orbitals involved in the lowest energy excitation of the dicationic, cationic, and neutral species of unsubstituted 1,4- (left) and 1,3- (right) PBBs are compared for the EOM-CCSD and TD-CAM-B3LYP methods.

polyarylpyridiniums. This qualitative disagreement is to be considered in conjunction with the quantitative disagreement for the cationic excitation energies discussed in section 9.3 and shown in Tables 4 and 5. Analysis of the first several excited states with both CC and TD-DFT approaches shows that these states all have significant charge transfer character. Thus it is expected that disagreement between CC and DFT cationic energies is a consequence of this charge transfer character.

As a final point of discussion we point out a heretofore unaddressed observation from our electronic structure calculations, which is the unusually small energy gap between the S_0 and T_1 ground electronic states of 1,4- PBBs at the Franck-Condon geometry. These values are listed for comparison in Table 10. With both DFT and CC approaches the gap between these two states is predicted to be less than 0.5 eV. The energy gap is under-predicted by DFT, which is useful for analysis of the error in DFT in larger, substituted systems. Table 11 shows the S_0-T_1 energy gap for all 1,4- PBBs in the present study. A small S_0-T_1 energy gap would be advantageous for a variety of applications in spintronics. The small energy gaps in 1,4- PBBs suggest that they may be uniquely suitable for such applications.

Compound	**S_0-T_1 gap (eV)**
unsubstituted (IP-EOM/EOM-CCSD)	0.476
unsubstituted (TD-CAM-B3LYP)	0.280
methylated	0.421
R=Phenyl	0.132
R=Pyridyl	0.141
R=Butyl	0.167

Table 11: The energy gap between the ground singlet and triplet electronic states is shown for all of the 1,4- bridged compounds in the present study.

9.6 References

[1] M.S. Whittingham, MRS Bull., 33 (2008) 411-419.
[2] J. Fortage, C. Peltier, C. Perruchot, Y. Takemoto, Y. Teki, F. Bedioui, V. Marvaud, G. Dupeyre, L. Pospisil, C. Adamo, M. Hromadova, I. Ciofini, P.P. Laine, J. Am. Chem. Soc., 134 (2012) 2691-2705.
[3] X.-P. Gao, H.-X. Yang, Energy Environ. Sci., 3 (2010) 174-189.
[4] A. Funston, J.P. Kirby, J.R. Miller, L. Pospisil, J. Fiedler, M. Hromadova, M. Gal, J. Pecka, M. Valasek, Z. Zawada, P. Rempala, J. Michl, J. Phys. Chem. A, 109 (2005) 10862-10869.
[5] M. Valasek, J. Pecka, J. Jindrich, G. Calleja, P.R. Craig, J. Michl, J. Org. Chem., 70 (2005) 405-412.
[6] I.S. Ufimtsev, T.J. Martinez, J. Chem. Theory Comput., 4 (2008) 222-231.
[7] I.S. Ufimtsev, T.J. Martinez, J. Chem. Theory Comput., 5 (2009) 1004-1015.
[8] I.S. Ufimtsev, T.J. Martinez, J. Chem. Theory Comput., 5 (2009) 2619-2628.
[9] T. Yanai, D.P. Tew, N.C. Handy, Chem. Phys. Lett., 393 (2004) 51-57.
[10] M. Cossi, V. Barone, R. Cammi, J. Tomasi, Chem. Phys. Lett., 255 (1996) 327-335.
[11] V. Barone, M. Cossi, J. Tomasi, J. Chem. Phys., 107 (1997) 3210-3221.
[12] Y. Shao, Z. Gan, E. Epifanovsky, A.T.B. Gilbert, M. Wormit, J. Kussmann, A.W. Lange, A. Behn, J. Deng, X. Feng, D. Ghosh, M. Goldey, P.R. Horn, L.D. Jacobson, I. Kaliman, R.Z. Khaliullin, T. Kus, A. Landau, J. Liu, E.I. Proynov, Y.M. Rhee, R.M. Richard, M.A. Rohrdanz, R.P. Steele, E.J. Sundstrom, H.L. Woodcock, III, P.M. Zimmerman, D. Zuev, B. Albrecht, E. Alguire, B. Austin, G.J.O. Beran, Y.A. Bernard, E. Berquist, K. Brandhorst, K.B. Bravaya, S.T. Brown, D. Casanova, C.-M. Chang, Y. Chen, S.H. Chien, K.D. Closser, D.L. Crittenden, M. Diedenhofen, R.A. DiStasio, Jr., H. Do, A.D. Dutoi, R.G. Edgar, S. Fatehi, L. Fusti-Molnar, A. Ghysels, A. Golubeva-Zadorozhnaya, J. Gomes, M.W.D. Hanson-Heine, P.H.P. Harbach, A.W. Hauser, E.G. Hohenstein, Z.C. Holden, T.-C. Jagau, H. Ji, B. Kaduk, K. Khistyaev, J. Kim, J. Kim, R.A. King, P. Klunzinger, D. Kosenkov, T. Kowalczyk, C.M. Krauter, K.U. Lao, A.D. Laurent, K.V. Lawler, S.V. Levchenko, C.Y. Lin, F. Liu, E. Livshits, R.C. Lochan, A. Luenser, P. Manohar, S.F. Manzer, S.-P. Mao, N. Mardirossian, A.V. Marenich, S.A. Maurer, N.J. Mayhall, E. Neuscamman, C.M. Oana, R. Olivares-Amaya, D.P. O'Neill, J.A. Parkhill, T.M. Perrine, R. Peverati, A. Prociuk, D.R. Rehn, E. Rosta, N.J. Russ, S.M. Sharada, S. Sharma, D.W. Small, A. Sodt, T. Stein, D. Stueck, Y.-C. Su, A.J.W. Thom, T. Tsuchimochi, V. Vanovschi, L. Vogt, O. Vydrov, T. Wang, M.A. Watson, J. Wenzel, A. White, C.F. Williams, J. Yang, S. Yeganeh, S.R. Yost, Z.-Q. You, I.Y. Zhang, X. Zhang, Y. Zhao, B.R. Brooks, G.K.L. Chan, D.M. Chipman, C.J. Cramer, W.A. Goddard, III, M.S. Gordon, W.J. Hehre, A. Klamt, H.F. Schaefer, III, M.W. Schmidt, C.D. Sherrill, D.G. Truhlar, A. Warshel, X. Xu, A. Aspuru-Guzik, R. Baer, A.T. Bell, N.A. Besley, J.-D. Chai, A. Dreuw, B.D. Dunietz, T.R. Furlani, S.R. Gwaltney, C.-P. Hsu, Y. Jung, J. Kong, D.S. Lambrecht, W. Liang, C. Ochsenfeld, V.A. Rassolov, L.V. Slipchenko, J.E. Subotnik, T. Van Voorhis, J.M. Herbert, A.I. Krylov, P.M.W. Gill, M. Head-Gordon, Mol. Phys., 113 (2015) 184-215.
[13] R.L. Martin, J. Chem. Phys., 118 (2003) 4775-4777.
[14] V.N. Staroverov, E.R. Davidson, J. Am. Chem. Soc., 122 (2000) 186-187.
[15] V.N. Staroverov, E.R. Davidson, Chem. Phys. Lett., 330 (2000) 161-168.
[16] J.F. Stanton, R.J. Bartlett, J. Chem. Phys., 98 (1993) 7029-7039.
[17] M. Nooijen, R.J. Bartlett, J. Chem. Phys., 102 (1995) 3629-3647.
[18] S. Hirata, M. Nooijen, R.J. Bartlett, Chem. Phys. Lett., 328 (2000) 459-468.

[19] P. Piecuch, S.A. Kucharski, K. Kowalski, M. Musial, Comput. Phys. Commun., 149 (2002) 71-96.
[20] J.R. Gour, P. Piecuch, M. Wloch, J. Chem. Phys., 123 (2005).
[21] J.R. Gour, P. Piecuch, J. Chem. Phys., 125 (2006).
[22] M.S. Gordon, M.W. Schmidt, Theory and Applications of Computational Chemistry: the First Forty Years, (2005) 1167-1189.
[23] A. Dreuw, M. Head-Gordon, J. Am. Chem. Soc., 126 (2004) 4007-4016.
[24] J.J. Eriksen, S.P.A. Sauer, K.V. Mikkelsen, O. Christiansen, H.J.A. Jensen, J. Kongsted, Mol. Phys., 111 (2013) 1235-1248.